Cell-Membrane-Mimicking Lipid-Coated Nanoparticles Confer Raman Enhancement to Membrane Proteins and Reveal Membrane-Attached Amyloid-β Conformation

Debanjan Bhowmik,[†] Kaustubh R. Mote,[‡] Christina M. MacLaughlin,[§] Nupur Biswas,[⊥] Bappaditya Chandra,[†] Jaydeep K. Basu,[⊥] Gilbert C. Walker,[§] Perunthiruthy K. Madhu,[*,†,‡] and Sudipta Maiti[*,†]

[†]Department of Chemical Sciences, Tata Institute of Fundamental Research, Homi Bhabha Road, Colaba, Mumbai 400005, India, [‡]TIFR Centre for Interdisciplinary Sciences, 21 Brundavan Colony, Narsinghi, Hyderabad 500075, India, [§]Department of Chemistry, Lash Miller Laboratories, University of Toronto, Toronto, ON M5S 3H6, Canada, and [⊥]Department of Physics, Indian Institute of Science, Bengaluru 560012, India

ABSTRACT Identifying the structures of membrane bound proteins is critical to understanding their function in healthy and diseased states. We introduce a surface enhanced Raman spectroscopy technique which can determine the conformation of membrane-bound proteins, at low micromolar concentrations, and also in the presence of a substantial membrane-free fraction. Unlike conventional surface enhanced Raman spectroscopy, our approach does not require immobilization of molecules, as it uses spontaneous binding of proteins to lipid bilayer-encapsulated Ag nanoparticles. We apply this technique to probe membrane-attached oligomers of Amyloid-β_{40} (Aβ_{40}), whose conformation is keenly sought in the context of Alzheimer's disease. Isotope-shifts in the Raman spectra help us obtain secondary structure information at the level of individual residues. Our results show the presence of a β-turn, flanked by two β-sheet regions. We use solid-state NMR data to confirm the presence of the β-sheets in these regions. In the membrane-attached oligomer, we find a strongly contrasting and near-orthogonal orientation of the backbone H-bonds compared to what is found in the mature, less-toxic Aβ fibrils. Significantly, this allows a "porin" like β-barrel structure, providing a structural basis for proposed mechanisms of Aβ oligomer toxicity.

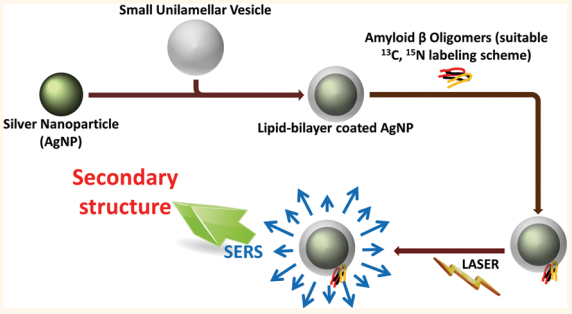

KEYWORDS: amyloid beta peptide · oligomers · surface enhanced Raman spectroscopy · membrane protein structures · solid-state NMR · lipid SERS · lipid-coated nanoparticles

A key feature of many protein-aggregation linked human diseases, such as Alzheimer's (AD), Parkinson's, and Type II diabetes, is the existence of a small soluble aggregate species which displays strong affinity to cell membranes.[1−3] The structure of the species[4] and the nature of its interaction with membranes have therefore attracted intense scrutiny.[5] In the case of Alzheimer's amyloid-β, some solution-state structural parameters of the early oligomeric species[6,7] have been obtained recently. Oligomers are the smallest aggregates (n-mers with $n < 10$) to display a high affinity for lipid bilayers, and are possibly key species in the toxic cascade of this extracellular peptide.[8,9] These data suggest an overall structural topology similar to the less toxic mature fibrils, with significant differences in specific segments. Unfortunately, very little is known about the conformation of these early oligomers in the lipid bilayer (though some structural parameters of larger aggregates in the membrane have been reported[10]).

There are several challenges to learning the membrane bound oligomer conformations. Most notably, the low concentrations of this species, and the simultaneous presence of other low membrane-affinity species (such as the monomers) in the solution, make this problem difficult to address with

* Address correspondence to madhu@tifr.res.in, maiti@tifr.res.in.

Received for review May 26, 2015 and accepted August 18, 2015.

Published online August 25, 2015
10.1021/acsnano.5b03175

conventional techniques such as solution-state NMR and CD. Solid-state NMR (following flash freezing and lyophilization of the oligomeric solution) can yield information about some secondary structural elements (such as α-helix/β-sheet), but it is difficult to discern some others (such as β-turns). Resistive pulse sensing methods have identified the size of the oligomers, but do not report on oligomer structure.[11] Plasmonic particles have been used previously to probe amyloid-β aggregation,[12] but this study did not probe the aggregate interaction with membranes or the aggregate structure.

Our solution to overcome the challenges and limitations of earlier methods includes the following elements. First, we employ Raman spectroscopy, which has been used widely as a label-free method to investigate the structures of peptides and proteins[13] and furthermore use Surface Enhanced Raman Spectroscopy (SERS) from silver nanoparticles (AgNPs) to take advantage of surface plasmons that enhance the scattering of protein vibrations. Second, we integrate a recently developed technique[14] to encapsulate AgNPs with a lipid bilayer in aqueous solutions. While they were originally used to provide stability to the SERS nanoparticle labels, here we take the novel approach of using them as cell membrane mimics with plasmonic properties. Third, we incubate the peptide of interest with these particles, and allow them to spontaneously attach to the lipid membrane.

The combined strategy confers important advantages. The plasmon enhancement is expected to be strongly localized within a few nanometers from the nanoparticle surface.[15] Thus, only the species which are bound to the lipid bilayer coating would experience the SERS effect and the free population in solution would not. This strategy also helps avoid artifacts associated with the alternate technique of immobilization of peptides on nanoparticles and decreases spectral background contributions from unbound solution species.

We have chosen this new method to probe small membrane-attached oligomers (*n*-mers with $n < 10$) of Alzheimer's Aβ_{40}. We have used isotope-shifts in the Raman spectra to obtain secondary structure information at the level of individual residues. Where possible, we have independently verified predictions using solid-state NMR spectroscopy.

Our results show the presence of a β-turn, flanked by two β-sheet regions in the membrane attached oligomers. We find a near-orthogonal orientation of the backbone H-bonds compared to the mature, less-toxic Aβ fibrils. Significantly, this allows a "porin" like β-barrel structure, providing a structural basis for proposed mechanisms of toxicity.

RESULTS AND DISCUSSION

Lipid bilayer coating of AgNPs is confirmed by TEM imaging (Figure 1A). The width of the surface layer (4.1 ± 0.6 nm, $n = 49$, Figure S1A) is consistent with that of a lipid bilayer. We also observe a Raman peak in the 2900 cm^{-1} region, which is characteristic of the C−H stretch of the lipid (Figure S2B).[16] There are no major peaks in the 1550−1750 cm^{-1} region, which is important for the determination of protein secondary structures (Figure S2A). Additional evidence of lipid encapsulation comes from the high stability of this suspension in a high salt containing (100 mM NaCl) solution (data not shown).

We first demonstrate our method by investigating the honey bee toxin, melittin. This protein has strong

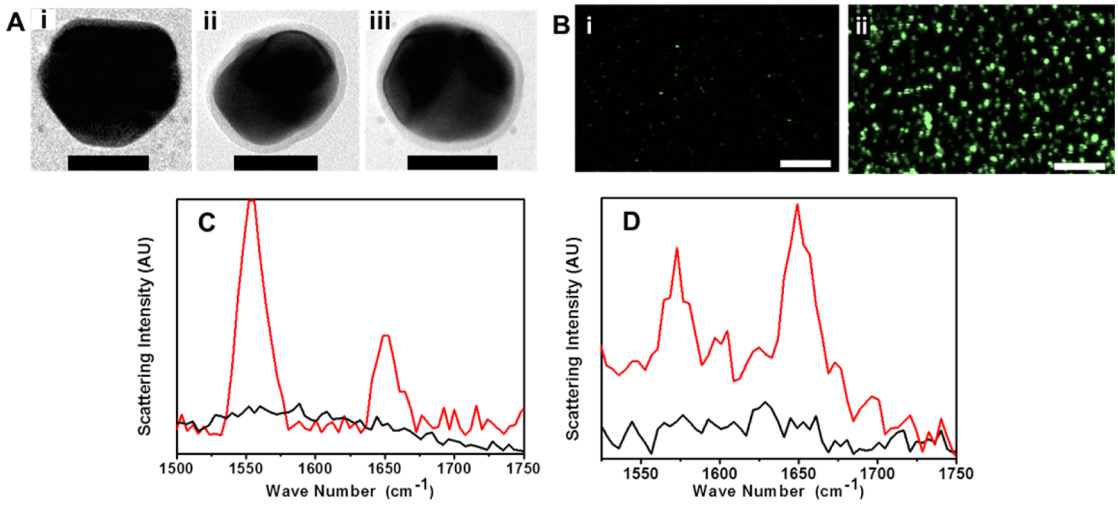

Figure 1. (A) TEM image of silver nanoparticles: (i) before and (ii) after coating with lipid bilayer; (iii) after incubating coated nanoparticles with Amyloid β oligomers. Lipid coating is visible as an extra layer around the particles. Scale bar is 50 nm. (B) Binding of N-terminal fluorescein labeled Aβ_{40} (FAβ_{40}) oligomers to lipid bilayer coated AgNPs: confocal image of bilayer coated AgNPs (i) before and (ii) after incubation with 2 μM of FAβ_{40} oligomers. Excitation: 488 nm. Emission: 500−600 nm. Scale bar: 5 μm. (C) SERS spectrum of melittin, in the presence of lipid encased AgNPs (red), and in the presence of bare AgNPs (black). (D) SERS spectrum of gramicidin A, in the presence of lipid encased AgNPs (red), and in the presence of bare AgNPs (black).

affinity for lipid bilayers and forms tetrameric α-helical structures in membrane.[17−20] Its Raman spectrum shows an α-helix signature at ∼1648 cm^{-1}. Another peak at ∼1549 cm^{-1} is assigned to side-chain tryptophan vibration and/or backbone amide II vibrations.[20] Our SERS experiment with ∼2 μM of melittin incubated with lipid-encapsulated Ag nanoparticles clearly shows these two peaks at 1648 and 1552 cm^{-1} (Figure 1C). Next, we investigate the considerably more complex structure of the water channel protein gramicidin A. This protein has high affinity to membranes, and the crystal structure and the Raman spectra are well studied. Its Raman spectrum has an Amide I signature at ∼1650 cm^{-1}[21] and an Amide II band (calculated) at ∼1570 cm^{-1},[22] which, taken together, are manifestations of the $\beta^{6.3}$-helix, a special structure only possible with alternate D/L-peptides. Our SERS experiment with 2 μM of gramicidin A incubated with lipid-encapsulated nanoparticles shows clear peaks at 1650 and 1573 cm^{-1} (Figure 1D). The SERS spectra obtained from the two unrelated membrane proteins using our method are completely consistent with the reported data. This demonstrates the capability of our method to deduce the secondary structure of membrane associated proteins using Raman structural markers. In our experiment, the sensitivity for the membrane associated fraction is much higher than conventional Raman, and we are able to probe proteins at 2 μM concentration.

While conventional Raman can be used for melittin and gramicidin A, as they can be prepared at much larger concentrations, the same is not true for many other important peptides, such as the aggregation-prone Amyloid-β. Determining the structure of the Amyloid β_{40} ($A\beta_{40}$) oligomers in the membrane bound state is important in the context of Alzheimer disease. An increase in the ion-permeability of the membranes is one of the consistently observed effects of this extracellular peptide.[23] Its conformation in the bilayer may therefore explain the subsequent deleterious effects on the cell, and help in developing effective drug candidates for AD. Fluorescence correlation spectroscopy (FCS), in different instrumentation formats,[24−26] with or without labeling dyes,[27] has been shown to be an effective tool for probing aggregation of proteins and peptides, including $A\beta_{40}$.[24,27−29] With the use of FCS, it has recently been shown that the oligomeric population present in an $A\beta$ solution displays the ability to attach to neuronal cell membranes.[8,30] FCS studies with lipid vesicles have also shown that this oligomeric population spontaneously attaches to the Small Unilamellar Vesicles (SUVs) composed of an equimolar mixture of POPC, POPG, and cholesterol, while the monomeric population does not.[9] The same ternary lipid mixture also constitutes the coating on the AgNPs, so we may expect that these oligomers would spontaneously bind to the bilayer-encased nanoparticles. We verify this binding by separate imaging studies with fluorescently labeled $A\beta_{40}$ oligomers incubated with these nanoparticles. These are small oligomers (*n*-mers with $n < 10$) prepared as described in ref 9 and separately tested by FCS to attach to lipid bilayer vesicles (data not shown). We have also demonstrated earlier that the oligomers, after attachment to cellular lipid bilayer membranes, do not dissociate into monomers.[30] Confocal microscopy of nanoparticles precipitated on the cover glass shows that the peptides attach to these lipid coated nanoparticles, and the presence of the metal core does not inhibit attachment (Figure 1B). $A\beta$ exposure, especially at high concentrations, can disturb lipid bilayers. Though we use lower concentrations (1 μM), we still verify the stability of the lipid bilayer upon $A\beta$ incubation using TEM (Figure 1A, iii). An analysis of TEM images shows that the 4.1 ± 0.6 nm thick lipid bilayer remains unchanged (4.2 ± 0.7 nm, $n = 49$, Figure S1B) after $A\beta$ incubation (Figure 1A, iii), suggesting that the bilayer is not significantly disturbed by $A\beta$.

We have previously shown that $A\beta_{40}$ provides adequate SERS signals, even at low concentrations, when chemically bonded to AgNPs.[31] However, for the membrane attached $A\beta_{40}$ species, a consistent enhancement in SERS can only be expected if the peptide inserts into the membrane to a distance that is close to the AgNP surface. There are conflicting views on whether $A\beta$ inserts deep into the membrane, perhaps because insertion depends on the type of oligomers and the nature of the membranes.[32−34] We therefore separately test the insertion in our case with X-ray reflectivity (XR) measurements,[35] which provides electron density profile (EDP) along the membrane thickness,[36,37] using similar membranes supported on silicon substrates before and after incubation with these oligomers, as described in the Supporting Information. Extracted EDP shows enhancement of film thickness as well as an increased density of the inner headgroup, which is a clear indication of the penetration of $A\beta$ peptides into the lipid membrane all the way down to the membrane−silicon substrate interface (Figure 2). We therefore expect reasonable signal intensity from $A\beta$ oligomers attached to the lipid bilayer encased nanoparticles.

We then performed SERS experiment of membrane coated AgNPs incubated with a mixture of small $A\beta$ oligomers. We find two prominent peaks in the Amide I region at 1665 cm^{-1} (with a shoulder at 1650 cm^{-1}), and at 1689 cm^{-1} (Figure 3A, black curve). The peak at 1689 cm^{-1} provides a strong indication of the presence of β-turn(s). A "β-turn" is also expected to have a weak to medium intensity band at ∼1665 cm^{-1} and a strong intensity band at ∼1650 cm^{-1}.[38] Thus, the peak at 1665 cm^{-1} and the shoulder at 1650 cm^{-1} can both have contributions from the β-turn. However, a peak at 1665 cm^{-1} may also have contribution from β-sheet structures,[38] and a peak at 1650 cm^{-1} may have contribution from α-helices.[38] We differentiate between these possibilities using the isotopic labeling technique

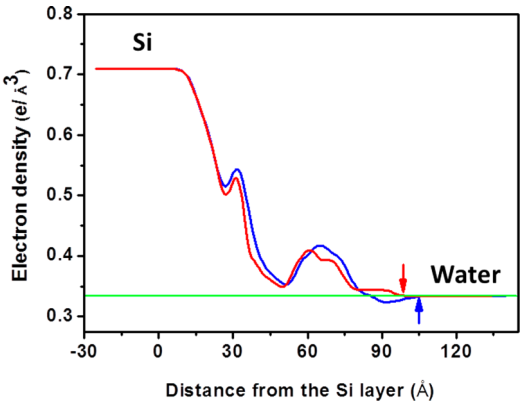

Figure 2. EDP (electron density profile) of the lipid membrane along its thickness, as obtained from X-ray reflectivity, before (red) and after (blue) incubation with Aβ. Arrows indicate the position of the lipid-bulk water interface before (red) and after (blue) Aβ incubation. Green line indicates bulk water electron density. Film thickness and electron densities of the layers increased after incubation with 1 μM of Aβ.

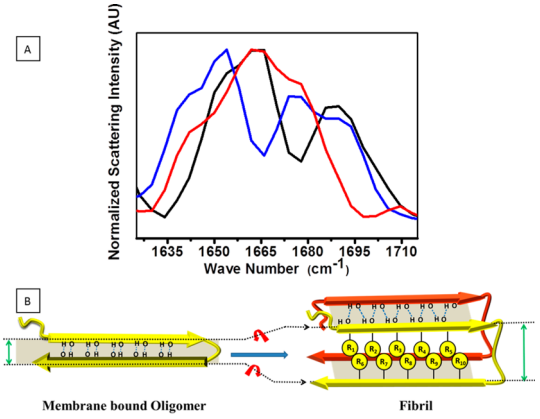

Figure 3. (A) Amide I region of SERS spectra of lipid membrane bound Aβ_{40}. Black, unlabeled Aβ_{40}; red, Aβ_{40} with ^{13}C and ^{15}N labeled D23 and K28 amino acids; blue, Aβ_{40} with ^{13}C and ^{15}N labeled E11, F19, A30, L34, V36 and G38 amino acids. (B) Cartoon showing the backbone reorientation required to form intermolecular parallel β-sheet structure in the fibrils, starting from an intramolecular antiparallel β-sheet structure in the membrane-bound oligomers, which contain a β-turn.

(see later). We infer that the peptide contains β-turn(s), perhaps together with other secondary structural elements.

We note that the free peptides present in the solution make negligible contribution to the Raman spectrum. Even at the 200 μM concentration and even at 10 times higher laser power (~9 mW), the peptide solution (without nanoparticles) does not show any discernible features in the Raman spectrum (data not shown). The contribution from the membrane attached peptides is therefore at least 3 orders of magnitude higher than that of the free peptides present in the solution. We also checked if the AgNP curvature has any effect on the structure of the membrane bound Aβ. SERS experiments with smaller particles (present in the supernatant after mild centrifugation) yield similar results to those obtained with larger particles, but with a reduced signal-to-noise ratio (Figure S6).

SERS by itself does not provide residue-level information about the location of specific secondary structural elements. This can be probed with isotopic substitutions,[39] which shift the vibrational frequencies of the Raman peaks. We use two different isotopic labeling sequences (isotopic sequence 1 and isotopic sequence 2, described later) to probe the local secondary structures of membrane bound Aβ oligomers. We note that partial isotopic substitution can drastically alter the Infrared (IR) absorption spectra, but Raman spectra appear to be less perturbed, other than the isotope-induced shift.[40] Secondary structure prediction by the Chou-Fasman algorithm[41] indicates possible β-turns in the Aβ_{40} sequence near residues A2, S8, Q15, E22, S26 and K28. Among these, predictions about S8 and S26 are unambiguous.[41] Since the N-terminal (residues 1−9) region has been found to be disordered both in the solution-state oligomers and in the mature fibrils,[7] we chose to investigate the S26 region by introducing isotopically labeled residues at the 23rd and the 28th positions of Aβ_{40} (called isotopic labeling "Sequence 1"). We find that the majority of the intensity of the 1689 cm^{-1} peak shifts to ~1678 cm^{-1} and the shoulder at 1650 cm^{-1} shifts to 1642 cm^{-1} (Figure 3A, red curve), but there are comparatively smaller changes for the 1665 cm^{-1} peak. This indicates that this region of the peptide contains a β-turn structure. A shift in the 1650 cm^{-1} peak to a lower wavenumber (1642 cm^{-1}) indicates that the 1650 cm^{-1} peak is also caused by the β-turn, and confirms the absence of significant amounts of α-helical content. Also, lack of substantial changes for the 1665 cm^{-1} peak upon isotopic substitution in the turn region indicates that this peak is primarily due to β-sheet structures present elsewhere in the sequence.

We then used isotopic labeling at positions E11, F19, A30, L34, V36, and G38 (Aβ_{40}, isotopic labeling "Sequence 2"). This particular labeling scheme was chosen as all these amino acids are shown to be part of two β-sheets flanking the turn region (residues 23−28) both in the mature fibrillar aggregate and in the soluble small oligomers.[7,42] We find that the 1665 cm^{-1} peak loses intensity; however, a new peak arises in the 1642 cm^{-1} region (Figure 3A, blue curve), consistent with an isotope-induced shift of the 1665 cm^{-1} peak. The peak at ~1650 cm^{-1} (consistent with a β-turn) does not shift or significantly decrease in intensity. This indicates that the region which has a β-sheet character in the oligomer in solution also has a similar character in the membrane attached oligomer. The peak at 1689 cm^{-1} broadens, indicating some amount of isotopic effect in the β-turn structural signature as well. This possibly indicates that A30 is close to the β-turn region.

We note that the observed signal can in principle arise from a direct peptide−nanoparticle interaction,

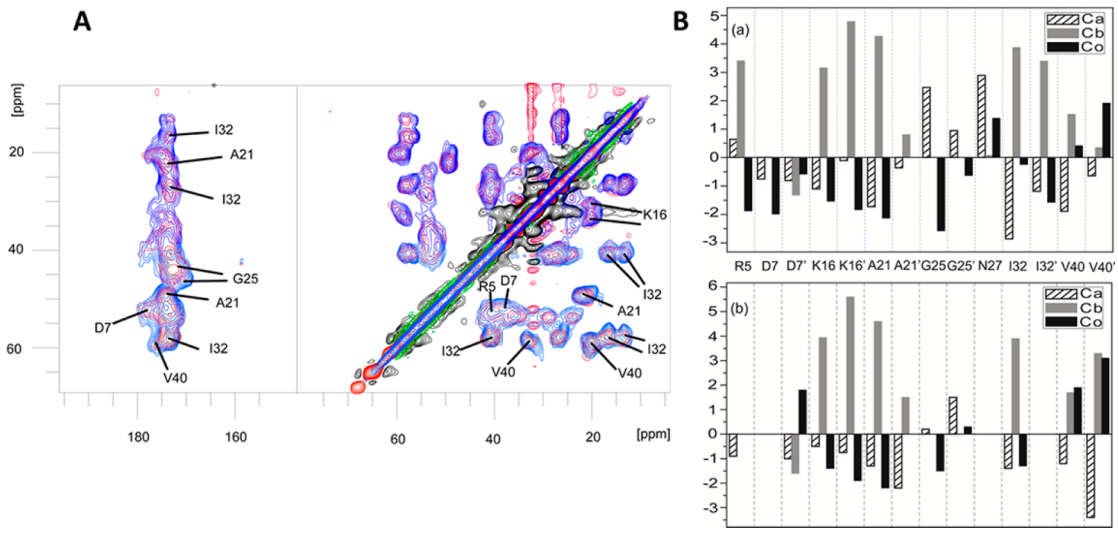

Figure 4. (A) Overlay of 2D $^{13}C-^{13}C$ PARIS-xy (m = 1) (N = 0.5) spectrum of Aβ_{40} fibrils (positive contours blue; negative contours green) and Aβ_{40} in lipid bound form (positive contours red; negative contours black) recorded with a mixing time of 100 ms. (B) Secondary ^{13}C chemical shifts calculated for Aβ_{40} fibrils (upper panel: a) and Aβ_{40} in lipid bound form (lower panel: b). The ordinate represents the difference in observed and random-coil Ca (hatched bars), Cb (gray bars), and Co (solid bars) chemical shifts for the uniformly labeled ^{13}C- and ^{15}N-amino acids in both the cases.

which if strong enough can also alter the peptide conformation. However, in absence of the lipid bilayer coating, incubation of Aβ oligomers in a nonaggregating nanoparticle solution does not yield any measurable Raman signal. On the other hand, C-terminal cysteine labeled Aβ (Aβ_{1-40}-Cys, which permits a Cys−Ag bond formation) does provide adequate signal under similar conditions (data not shown). This shows that interaction of unmodified Aβ with the nanoparticle is weak at best, and our signal is unlikely to have contributions from direct Aβ−Ag interactions.

Some of these predicted structural features of membrane bound Aβ oligomers can be verified by solid-state NMR, using the flash freezing and lyophilization technique demonstrated by us earlier.[7] A sample prepared using this strategy is expected to have signals from the membrane-bound as well as the free peptides. To maximize the signal from the bound conformation, we used a lipid to peptide ratio of 75:1, which is expected to result in the majority of the peptide ending up in the membrane-bound state. This was confirmed using FCS, which showed that only small Aβ species (both vesicle-bound and free) are present in this solution before flash-freezing, and the percentage of lipid-bound Aβ is ≥70% (Figure S3). This is consistent with our earlier results.[9] We also performed TEM imaging of these samples before and after flash-freezing and lyophilization. We observed only the vesicles, without any large Aβ aggregates (Figure S4A,B). As a control, we let another membrane-Aβ sample (not used for NMR) mature for 4 days before freezing, and this sample clearly shows larger fibril like structures (Figure S4C). This confirms that our sample consisted mostly of membrane-bound Aβ oligomers.

We used 2D $^{13}C-^{13}C$ correlation (PARIX-xy with 100 ms mixing time)[43] to assign the secondary structure of Aβ in a sample with ^{13}C and ^{15}N isotopic labeling at positions R5, D7, K16, A21, G25, N27, I32, V40. A strong truncation artifact of the lipid $-CH_2$ can be seen at ∼32.2 ppm in the indirect dimension, so peaks falling in that particular chemical shift range are ignored. In the lipid-bound form, Aβ shows a trend of secondary structure similar to the fibrils (Figure 4A,B). K16, A21, and I32 are known to have β-sheet structure in fibrils, and in the early oligomers.[7] I32 has two β-sheet conformations in the fibril, while in the membrane-bound form, it takes only the minor conformation observed in the fibrils. Similarity of the secondary chemical shift suggests that in the membrane-bound form they (K16, A21, and I32) are also part of the β-sheet structure. Some of the other residues, such as R5, D7, and N27, show broad peaks, which make it difficult to assign the resonances accurately. Although it is not possible to establish the sense of the β-sheet (parallel or antiparallel) or the presence of a β-turn from this set of solid-state NMR data, it clearly confirms the presence of β-sheet in the same regions suggested by our SERS findings.

We note here that SERS provides information about the global protein conformation that is complementary to solid-state NMR (ssNMR). Our ssNMR data could verify our Raman predictions only for a specific part of the peptide, which is in a regular β-sheet architecture. It is silent about the existence of the beta turn. On the other hand, Raman provides characteristic peaks for almost all types of secondary structures. Therefore, Raman spectroscopy, supported in part by ssNMR, is able to discern the β-sheet−β-turn−β-sheet structure observed here.

DISCUSSION

The consensus structure of mature Aβ_{40} fibrils, which are supposed to be nontoxic or less-toxic,[44] also has a turn in the region of residues 23−28. However, unlike the oligomer structure proposed herein, this turn is not a β-turn. The turn observed in the mature Aβ-fibrils facilitates intermolecular H-bonding and intramolecular hydrophobic interactions,[45,46] which give rise to the well-known "cross-beta" (parallel, in-register β-sheets) architecture of the amyloid fibrils. However, the structure of the membrane bound oligomeric Aβ_{40} found here shows a β-turn in the region between residues 23 and 28, flanked by antiparallel β-sheets. The model most consistent with these observations would predict a structure with this β-turn facilitating the formation of intramolecular antiparallel β-sheets (Figure 3B). Thus, while differences in the local secondary structure content between fibrils and oligomers are rather subtle, this apparent similarity hides profound differences in the chain geometry. The oligomer displays a near 90° turn of the backbone about its own axis (schematic in Figure 3B depicts this rotation) and the formation of intramolecular hydrogen bonds. This would bring the two arms of the same peptide much closer together than they are in the fibril.

It is interesting to speculate that such conformations are already present in the solution-state oligomers, even before they bind to the membrane. Structural parameters of spontaneously formed solution-state oligomers identified earlier[7] are consistent with the model proposed here, though they are not known in enough detail to provide a direct confirmation. However, a conformation similar to our model has been strongly suggested by simulation studies, solid-state NMR experiments performed with an engineered variant of Aβ, and studies with antibody-bound oligomers.[47−50] CD and IR spectra of Aβ in bilayers,[33,51] recorded at much higher concentrations where small oligomers are likely to be unstable,[6] also suggest a β-sheet rich structure in the membrane (though in some cases these β-sheets are observed to transform to α-helices).[33] Simulations of Aβ in the membrane have suggested both α-helical[52] and β-sheet rich structures, with the parallel intermolecular hydrogen bonded β-sheets similar to those of the fibril.[53] Our observations are at variance with such models.

We note that a dominant hypothesis about the mechanism of Aβ toxicity suggests that small oligomers assemble in the membrane to form an unregulated ion channel or a "pore".[54] The resultant disturbance of the ionic homeostasis across the neuronal membrane causes neuronal malfunction and, ultimately, neuronal death. However, the only membrane spanning β-sheet rich structures known to form transmembrane pores belong to the family of "porins".[55] They have antiparallel β-sheets joined by β-turns. Our observation of the β-sheet−β-turn−β-sheet architecture of Aβ oligomers in the membrane provides experimental evidence for such a conformation.

CONCLUSION

In conclusion, using a novel SERS technique, we show that there is a significant difference in the structural organization of the membrane-bound Aβ oligomers and fibrils. The presence of the β-sheet−β-turn−β-sheet motif observed here may be crucial for understanding the differences in the toxic properties of these two species. Our SERS approach also offers a window into the performance of therapeutic nanoparticles that capture Aβ oligomers[56] and artificial nanopores.[57] In addition, our cell-membrane-mimicking SERS nanoparticle construct can potentially determine the conformations of a broad range of membrane-associated molecules, without requiring high concentrations or surface immobilization.

EXPERIMENTAL SECTION

Silver Nanoparticle Synthesis. One millimolar $AgNO_3$ solution (50 mL) was heated to boiling in a 500 mL round-bottom flask, and 1 mL of the trisodiumcitrate solution (from a stock solution of 0.114 g in 10 mL of water) was added to it. After 45 min of reflux, the solution was cooled to obtain the nanoparticle solution. $AgNO_3$ was purchased from Merck (Schuchardt, Germany), and trisodium citrate was purchased from Sigma-Aldrich, Inc. (St. Louis, MO).

Peptide Synthesis. All the Aβ_{40} peptides (^{13}C labeled and unlabeled) used here were synthesized, purified, and characterized in the laboratory. The peptides were synthesized in an automated solid phase peptide synthesizer (PS3, Protein Technologies, Inc. Tucson, AZ) using 9-fluorenylmethoxycarbonyl (Fmoc) chemistry. All the Fmoc amino acids and reagents were purchased from Merck (Schuchardt, Hohenbrunn, Germany). Isotopically labeled Fmoc amino acids were purchased from CortecNet (Voisins-Le-Bretonneux, France).

Preparation and Characterization of Oligomers. Stock solutions (pH 10.5, 100 μM) of Aβ_{40} were diluted to a concentration of 2 μM by pH 7.4 phosphate buffer (buffer composition: 20 mM Na_2HPO_4, 150 mM NaCl, 5 mM KCl, pH adjusted to 7.4). These solutions were incubated for 30 min, to obtain small oligomer-rich solutions. The size and membrane affinity of the small oligomers were measured using Fluorescence Correlation Spectroscopy (FCS), as described earlier.[9]

Preparation of SERS Samples. A thin film of lipid was produced by mixing POPC (1-palmitoyl-2-oleoyl-*sn*-glycero-3-phosphocholine), POPG (1-palmitoyl-2-oleoyl-*sn*-glycero-3 phosphoglycerol), and cholesterol in equal molar ratios (PPC111; 15 mg in total) in chloroform, followed by drying under nitrogen stream. Remaining chloroform was removed under vacuum.

Silver nanoparticles were synthesized in the lab as described earlier. To coat lipid bilayers on AgNPs, first 8 mL of the silver nanoparticle (AgNPs) solution was centrifuged and the supernatant was discarded. Then, the precipitate was resuspended in 1 mL of distilled water and vortexed in the presence of PPC111 (15 mg). The mixture was then sonicated for 20 min in a water bath sonicator. The process of sonication coats a lipid bilayer on top of AgNPs. These coated AgNPs were tested to be stable

against salt. Coated AgNPs were separated by mild centrifugation (2000*g*, 12 min) followed by resuspension in phosphate buffer. The oligomeric solution of Aβ_{40} was then mixed with lipid bilayer coated AgNP solution. Aβ oligomers were allowed to interact with the lipid bilayer coat for 3 h. Immediately after the incubation period, SERS experiments were performed.

SERS Measurements. The Gramicidin A solution was allowed to incubate with the coated AgNPs for 6 h before experiments. All the Aβ_{40} solutions and mellitin solution were incubated with the AgNPs for 3 h before experiments. Raman spectra were recorded with a Confocal Raman Microscope (Witec Alpha300 RS, Germany) by exciting at 532 nm using ~900 μW power and 30 s of integration time. A 50×, 0.55 NA Zeiss air objective was used and the emission was collected by a 100 μm diameter optical fiber in a confocal geometry.

Confocal Measurements. Confocal measurements were performed with a confocal microscope (LSM 710, Carl Zeiss, Germany) using a 40× water immersion objective. A 488 nm laser excitation was used, and the fluorescence was collected between 500 and 600 nm.

TEM Measurements. Ten microliters of the sample solutions (either AgNPs or Membrane bound Aβ) was added to carbon-coated 100 mesh copper grids (Electron Microscopy Sciences, Hatfield, PA). After 2−3 min of incubation, excess solvent was blotted with tissue paper, and the sample was subjected to 4−5 cycles of mild washing with milli-Q water. Sample staining was achieved by incubation with 0.1% of uranyl acetate for 5 min. The grids were dried under an infrared lamp and examined under a transmission electron microscope (LIBRA 120, EFTEM, Carl Zeiss, Germany).

For examination of the lyophilized sample, a small amount of the solid powder was resuspended in water before placing it on the carbon-coated 100 mesh copper grid.

Conflict of Interest: The authors declare no competing financial interest.

Supporting Information Available: The Supporting Information is available free of charge on the ACS Publications website at DOI: 10.1021/acsnano.5b03175.

Supplementary figures and additional details about ssNMR and XR experiment (PDF)

Acknowledgment. The research was supported by grants from Department of Biotechnology, India (Grant No. BT/53/NE/TBP/2010) to S.M., from ARCI, India (Grant No. ARCI/D/FAO/Nano/K-16/Canada/11) to S.M. and G.C.W., from Department of Science and Technology, India to J.K.B., and from NSERC, Canada to G.C.W. B.C. acknowledges CSIR-SPM-SRF fellowship. We acknowledge the help of Lalit Borde for TEM imaging, M. Deshmukh and J. Dasgupta for access to the Raman Spectrometer, G. Krishnamoorthy for his kind gift of melittin and gramicidin A, Saha Institute of Nuclear Physics, India, for facilitating the experiments at the Indian Beamline, Photon Factory, KEK, Japan and Dr. Velaga Srihari for his assistance during the XR experiment.

REFERENCES AND NOTES

1. Chiti, F.; Dobson, C. M. Protein Misfolding, Functional Amyloid, and Human Disease. *Annu. Rev. Biochem.* **2006**, *75*, 333–366.
2. Terzi, E.; Holzemann, G.; Seelig, J. Interaction of Alzheimer β-Amyloid Peptide(1−40) with Lipid Membranes. *Biochemistry* **1997**, *36*, 14845–14852.
3. Jayasinghe, S. A.; Langen, R. Membrane Interaction of Islet Amyloid Polypeptide. *Biochim. Biophys. Acta, Biomembr.* **2007**, *1768*, 2002–2009.
4. Kumar, S. T.; Meinhardt, J.; Fuchs, A. K.; Aümuller, T.; Leppert, J.; Büchele, B.; Knupfer, U.; Ramachandran, R.; Yadav, J. K.; Prell, E.; et al. Structure and Biomedical Applications of Amyloid Oligomer Nanoparticles. *ACS Nano* **2014**, *8*, 11042–11052.
5. Johnson, R. D.; Steel, D. G.; Gafni, A. Structural Evolution and Membrane Interactions of Alzheimer's Amyloid-beta Peptide Oligomers: New Knowledge from Single-molecule Fluorescence Studies. *Protein Sci.* **2014**, *23*, 869–883.
6. Nag, S.; Sarkar, B.; Chandrakesan, M.; Abhyanakar, R.; Bhowmik, D.; Kombrabail, M.; Dandekar, S.; Lerner, E.; Haas, E.; Maiti, S. A Folding Transition Underlies the Emergence of Membrane Affinity in Amyloid-β. *Phys. Chem. Chem. Phys.* **2013**, *15*, 19129–19133.
7. Sarkar, B.; Mithu, V. S.; Chandra, B.; Mandal, A.; Chandrakesan, M.; Bhowmik, D.; Madhu, P. K.; Maiti, S. Significant Structural Differences between Transient Amyloid-β Oligomers and Less-Toxic Fibrils in Regions Known To Harbor Familial Alzheimer's Mutations. *Angew. Chem., Int. Ed.* **2014**, *53*, 6888–6892.
8. Sarkar, B.; Das, A. K.; Maiti, S. Thermodynamically Stable Amyloid-β Monomers Have Much Lower Membrane Affinity than the Small Oligimers. *Front. Physiol.* **2013**, *4* (84), 1–11.
9. Bhowmik, D.; Das, A. K.; Maiti, S. Rapid Cell-Free Assay for Membrane-Active Forms of Amyloid-β. *Langmuir* **2015**, *31*, 4049–4053.
10. Qiang, W.; Yau, W. M.; Schulte, J. Fibrillation of β Amylloid Peptides in the Presence of Phospholipid Bilayers and the Consequent Membrane Disruption. *Biochim. Biophys. Acta, Biomembr.* **2015**, *1848*, 266–276.
11. Yusko, E. C.; Prangkio, P.; Sept, D.; Rollings, R. C.; Li, J. L.; Mayer, M. Single-Particle Characterization of A beta Oligomers in Solution. *ACS Nano* **2012**, *6*, 5909–5919.
12. Choi, I.; Lee, L. P. Rapid Detection of A beta Aggregation and Inhibition by Dual Functions of Gold Nanoplasmic Particles: Catalytic Activator and Optical Reporter. *ACS Nano* **2013**, *7*, 6268–6277.
13. Oladepo, S. A.; Xiong, K.; Hong, Z.; Asher, S. A.; Handen, J.; Lednev, I. K. UV Resonance Raman Investigations of Peptide and Protein Structure and Dynamics. *Chem. Rev.* **2012**, *112*, 2604–2628.
14. Ip, S.; MacLaughlin, C. M.; Gunari, N.; Walker, G. C. Phospholipid Membrane Encapsulation of Nanoparticles for Surface-Enhanced Raman Scattering. *Langmuir* **2011**, *27*, 7024–7033.
15. Siddhanta, S.; Narayana, C. Surface Enhanced Raman Spectroscopy of Proteins: Implications for Drug Designing. *Nanomater. Nanotechnol.* **2012**, *2*, 1–13.
16. Stewart, A. F.; Lee, A.; Ahmed, A.; Ip, S.; Kumacheva, E.; Walker, G. C. Rational Design for the Controlled Aggregation of Gold Nanorods *via* Phospholipid Encapsulation for Enhanced Raman Scattering. *ACS Nano* **2014**, *8*, 5462–5467.
17. Terwilliger, T. C.; Eisenberg, D. The Structure of Melittin. I. Structure Determination and Partial Refinement. *J. Biol. Chem.* **1982**, *257*, 6010–6015.
18. Terwilliger, T. C.; Eisenberg, D. The Structure of Melittin. II. Interpretation of the Structure. *J. Biol. Chem.* **1982**, *257*, 6016–6022.
19. Terwilliger, T. C.; Weissman, L.; Eisenberg, D. The Structure of Melittin in the Form I Crystals and its Implication for Melittin's Lytic and Surface Activities. *Biophys. J.* **1982**, *37*, 353–361.
20. Vogel, H.; Jahnig, F. The Structure of Melittin in Membranes. *Biophys. J.* **1986**, *50*, 573–582.
21. Naik, V. M.; Krimm, S. Vibrational Analysis of the Structure of Gramicidin A. II. Vibrational Spectra. *Biophys. J.* **1986**, *49*, 1147–1154.
22. Naik, V. M.; Krimm, S. Vibrational Analysis of the Structure of Gramicidin A. I. Normal Mode Analysis. *Biophys. J.* **1986**, *49*, 1131–1145.
23. Kayed, R.; Sokolov, Y.; Edmonds, B.; McIntire, T. M.; Milton, S. C.; Hall, J. E.; Glabe, C. G. Permeabilization of Lipid Bilayers is a Common Conformation-Dependent Activity of Soluble Amyloid Oligimers in Protein Misfolding Diseases. *J. Biol. Chem.* **2004**, *279*, 46363–46366.
24. Sengupta, P.; Garai, K.; Sahoo, B.; Callaway, D. J. E.; Maiti, S. The Amyloid β Peptide (Aβ_{1-40}) is Thermodynamically Soluble at Physiological Concentrations. *Biochemistry* **2003**, *42* (35), 10506–10513.
25. Garai, K.; Sureka, R.; Maiti, S. Detecting Amyloid-β aggregation with fiber based fluorescence correlation spectroscopy. *Biophys. J.* **2007**, *92* (7), L55–57.

26. Sahoo, B.; Nag, S.; Sengupta, P.; Maiti, S. On the Stability of the Soluble Amyloid Aggregates. *Biophys. J.* **2009**, *97* (5), 1454–1460.
27. Sahoo, B.; Balaji, J.; Nag, S.; Kaushalya, S. K.; Maiti, S. Protein Aggregation Probed by Two-photon Fluorescence Correlation Spectroscopy of Native Tryptophan. *J. Chem. Phys.* **2008**, *129*, 075103.
28. Tjernberg, L. O.; Pramanik, A.; Bjorling, S.; Thyberg, P.; Thyberg, J.; Nordstedt, C.; Berndt, K. D.; Terenius, L.; Rigler, R. Amyloid β-peptide Polymerization Studied Using Fluorescence Correlation Spectroscopy. *Chem. Biol.* **1999**, *6*, 53–62.
29. Nag, S.; Sarkar, B.; Bandyopadhyay, A.; Sahoo, B.; Sreenivasan, V. K. A.; Kombrabail, M.; Muralidharan, C.; Maiti, S. The Nature of the Amyloid-β Monomer and the Monomer-oligomer Equilibrium. *J. Biol. Chem.* **2011**, *286* (16), 13827–13833.
30. Nag, S.; Chen, J.; Irudayaraj, J.; Maiti, S. Direct Measurement of The Attachment and Assembly of Small Amyloid-β Oligomers on Live Cell Membranes at Physiological Concentrations. *Biophys. J.* **2010**, *99* (6), 1969–1975.
31. Bhowmik, D.; MacLaughlin, C. M.; Chandrakesan, M.; Ramesh, P.; Venkatramani, R.; Walker, G. C.; Maiti, S. pH Changes the Aggregation Property of Amyloid-β without Altering the Monomeric Conformation. *Phys. Chem. Chem. Phys.* **2014**, *16*, 885–889.
32. Lal, R.; Lin, H.; Quist, A. P. Amyloid Beta Ion Channel: 3D Structure and Relevance to Amyloid Channel Paradigm. *Biochim. Biophys. Acta, Biomembr.* **2007**, *1768*, 1966–1975.
33. Wong, P. T.; Schauerte, J. A.; Wisser, K. C.; Ding, H.; Lee, E. L.; Steel, D. G.; Gafni, A. Amyloid-beta Membrane Binding and Permeabilization are Distinct Processes Influenced Separately by Membrane Charge and Fluidity. *J. Mol. Biol.* **2009**, *386*, 81–96.
34. Curtain, C. C.; Ali, F. E.; Smith, D. G.; Bush, A. I.; Masters, C. L.; Barnham, K. J. Metal Ions, pH, and Cholesterol Regulate the Interactions of Alzheimer's Disease Amyloid-β Peptide with Membrane Lipid. *J. Biol. Chem.* **2003**, *278*, 2977–2982.
35. Basu, J. K.; Sanyal, M. K. Ordering and Growth of Langmuir-Blodgett Films: X-ray Scattering Studies. *Phys. Rep.* **2002**, *363*, 1–84.
36. Bhattacharya, R.; Kanchi, S.; Roobala, C.; Lakshminarayanan, A.; Seeck, O. H.; Maiti, P. K.; Ayappa, K. G.; Jayaraman, N.; Basu, J. K. A New Microscopic Insight into Membrane Penetration and Reorganization by PETIM dendrimers. *Soft Matter* **2014**, *10*, 7577–7587.
37. Miller, C. E.; Majewski, J.; Gog, T.; Kuhl, T. L. Characterization of Biological Thin Films at the Solid-Liquid Interface by X-Ray Reflectivity. *Phys. Rev. Lett.* **2005**, *94*, 238104.
38. Krimm, S.; Bandekar, J. Vibrational Spectroscopy and Conformation of Peptides, Polypeptides, and Proteins. *Adv. Protein Chem.* **1986**, *38*, 181–364.
39. Moran, S. D.; Zanni, M. T. How to Get Insight into Amyloid Structure and Formation from Infrared Spectroscopy. *J. Phys. Chem. Lett.* **2014**, *5*, 1984–1993.
40. Welch, W. R. W.; Kubelka, J.; Keiderling, T. A. Infrared, Vibrational Circular Dichroism, and Raman Spectral Simulations for β-sheet Structures with Various Isotropic Labels, Interstrand, and Stacking Arrangements Using Density Functional Theory. *J. Phys. Chem. B* **2013**, *117*, 10343–10358.
41. Chou, P. Y.; Fasman, G. D. Prediction of Protein Conformation. *Biochemistry* **1974**, *13*, 222–245.
42. Mithu, V. S.; Sarkar, B.; Bhowmik, D.; Chandrakesan, M.; Maiti, S.; Madhu, P. K. Zn^{+2} Binding Disrupts the Asp^{23}-Lys^{28} Salt Bridge without Altering the Hairpin-Shaped Cross-β Structure of $A\beta_{42}$ Amyloid Aggregates. *Biophys. J.* **2011**, *101*, 2825–2832.
43. Weingarth, M.; Demco, D. E.; Bodenhausen, G.; Tekely, P. Improved Magnetization Transfer in Solid-state NMR with Fast Magic Angle Spinning. *Chem. Phys. Lett.* **2009**, *469*, 342–348.
44. McLean, C. A.; Cherny, R. A.; Fraser, F. W.; Fuller, S. J.; Smith, M. J.; Beyreuther, K.; Bush, A. I.; Masters, C. L. Soluble Pool of Abeta Amyloid as a Determinant of Severity of Neurogeneration in Alzheimer's Disease. *Ann. Neurol.* **1999**, *46*, 860–866.
45. Sawaya, M. R.; Sambashivan, S.; Nelson, R.; Ivanova, M. I.; Sievers, S. A.; Apostol, M. I.; Thompson, M. J.; Balbirnie, M.; Wiltzius, J. J.; McFarlane, H. T.; et al. Atomic Structures of Amyloid Cross-β Spines Reveal Varied Steric Zippers. *Nature* **2007**, *447*, 453–457.
46. Lin, Y. C.; Petersson, E. J.; Fakhraai, Z. Surface Effects Mediate Self-Assembly of Amyloid-beta Peptides. *ACS Nano* **2014**, *8*, 10178–10186.
47. Gu, L.; Liu, C.; Stroud, J. C.; Ngo, S.; Jiang, L.; Guo, Z. Antiparallel Triple-strand Architecture for Prefibrillar Aβ42 Oligomers. *J. Biol. Chem.* **2014**, *289*, 27300–27313.
48. Lendel, C.; Bjerring, M.; Dubnovitsky, A.; Kelly, R. T.; Filippov, A.; Antzutkin, O. N.; Nielsen, N. C.; Hard, T. A Hexameric Peptide Barrel as Building Block of Amyloid-β Protofibrils. *Angew. Chem., Int. Ed.* **2014**, *53*, 12756–12760.
49. Scheidt, H. A.; Morgado, I.; Huster, D. Solid-state NMR Reveals a Close Structural Relationship between Amyloid-β Protofibrils and Oligomers. *J. Biol. Chem.* **2012**, *287*, 22822–22826.
50. Labouze, J. N.; Nguyen, P. H.; Sterpone, F.; Berthoumieu, O.; Buchete, N. V.; Coté, S.; Simone, A. D.; Doig, A. J.; Faller, P.; Garcia, A.; et al. Amyloid β Protein and Alzheimer's Disease: When Computer Simulations Complement Experimental Studies. *Chem. Rev.* **2015**, *115*, 3518–3563.
51. de Planque, M. R.; Raussens, V.; Contera, S. A.; Rijkers, D. T.; Liskamp, R. M.; Ruysschaert, J. M.; Ryan, J. F.; Separovic, F.; Watts, A. β-Sheet Structured β-Amyloid(1−40) Perturbs Phosphatidylcholine Model Membranes. *J. Mol. Biol.* **2007**, *368*, 982–997.
52. Xu, Y.; Shen, J.; Luo, X.; Zhu, W.; Chen, K.; Ma, J.; Jiang, H. Conformational Transition of Amyloid β-Peptide. *Proc. Natl. Acad. Sci. U. S. A.* **2005**, *102*, 5403–5407.
53. Jang, H.; Zheng, J.; Lal, R.; Nussinov, R. New Structures Help the Modeling of Toxic Amyloid β Ion Channels. *Trends Biochem. Sci.* **2008**, *33*, 91–100.
54. Lin, H.; Bhatia, R.; Lal, R. Amyloid Beta Protein Forms Ion Channels: Implications for Alzheimer's Disease Pathophysiology. *FASEB J.* **2001**, *15*, 2433–2444.
55. White, S. H.; Wimley, W. C. Membrane Protein Folding and Stability: Physical Principles. *Annu. Rev. Biophys. Biomol. Struct.* **1999**, *28*, 319–365.
56. Song, Q. X.; Huang, M.; Yao, L.; Wang, X. L.; Gu, X.; Chen, J.; Chen, J.; Huang, J. L.; Hu, Q. Y.; Kang, T.; et al. Lipoprotein-Based Nanoparticles Rescue the Memory Loss of Mice with Alzheimer's Disease by Accelerating the Clearance of Amyloid-Beta. *ACS Nano* **2014**, *8*, 2345–2359.
57. Trick, J. L.; Wallace, E. J.; Bayley, H.; Sansom, M. S. P. Designing a Hydrophobic Barrier within Biomimetic Nanopores. *ACS Nano* **2014**, *8*, 11268–11279.